processes

MDPI

Article

Structural Characterization and High-Pressure Methane Adsorption Mechanism Across Different Coal Ranks: Insights from Molecular Modeling

Wanyuan Nie [1,2], Manli Huang [1,3,4,*], Tong Zhang [1,3] and Ming Cheng [2]

[1] China University of Mining and Technology, Xuzhou 221116, China
[2] School of Geology and Mining Engineering, Xinjiang University, Urumqi 830047, China
[3] School of Resources and Geosciences, China University of Mining and Technology, Xuzhou 221116, China
[4] Key Laboratory of Coalbed Methane Resources and Reservoir Formation Process, China University of Mining and Technology, Jinshan East Road, Xuzhou 221000, China
* Correspondence: tb24010002a41@cumt.edu.cn

Abstract

To elucidate coalbed methane (CBM) adsorption mechanisms in deep coal reservoirs, the macromolecular structures of coal samples with different coal ranks were characterized using FTIR, XPS, and C NMR, followed by the construction of corresponding molecular models. Grand Canonical Monte Carlo (GCMC) simulations were employed to investigate methane adsorption behavior within the coal matrix at 313.15 K and pressures up to 20 MPa. The results showed that as coal rank increased ($R_{o,max}$ = 1.63% to 3.18%), the coal macromolecular structure transformed from a side-chain-rich configuration to a highly aromatized and directionally stacked structure. This structural maturation leads to a more compact coal matrix, evidenced by a reduction in free volume from 5108.39 Å^3 to 3999.87 Å^3 and a decline in accessible free volume from 8.23% to 6.26%, thereby restricting the effective space for methane storage. At 20 MPa, although the pore walls of high-rank coal exhibit stronger localized adsorption capacity, the bulk adsorption capacity follows the order: DZ > ZC > SH. This suggests that under deep, high-pressure conditions, the pore-volume compression effect associated with increasing coal rank governs the upper limit of adsorption per unit mass of coal. As pressure increases into the deep reservoir regime, the state of methane in coal micropores gradually shifts from surface adsorption to a high-density, quasi-liquid filling behavior. Consequently, the influence of specific surface area diminishes, while effective free volume emerges as the primary determinant of high-pressure adsorption capacity. The impact of coal rank on deep methane adsorption reflects a competition between enhanced adsorption potential and restricted storage space. The densification-induced compression of effective free volume is identified as the dominant factor limiting the adsorption capacity of deep CBM. This study provides a molecular-scale understanding of deep CBM occurrence mechanisms and establishes a theoretical framework for resource evaluation.

Keywords: deep coalbed methane; coal rank; coal macromolecular structure; high-pressure methane adsorption; molecular simulation

Check for updates

Academic Editor: Chuanjin Yao

Received: 9 March 2026
Revised: 14 April 2026
Accepted: 22 April 2026
Published: 28 April 2026

Copyright: © 2026 by the authors. Licensee MDPI, Basel, Switzerland. This article is an open access article distributed under the terms and conditions of the Creative Commons Attribution (CC BY) license.

1. Introduction

Coalbed methane (CBM) is of significant strategic importance for optimizing the global energy structure, mitigating energy shortages, and reducing greenhouse gas emissions [1–4]. In recent years, as CBM exploration and development have progressively

extended to greater depths, coal reservoirs have been found to exhibit characteristics of elevated geothermal temperature, high reservoir pressure, and increased in situ stress [5–7]. Consequently, the occurrence and migration mechanisms of deep CBM differ markedly from those of shallow reservoirs, posing challenges to traditional understandings of CBM occurrence established under shallow-to-intermediate burial conditions.

CBM predominantly occurs in an adsorbed state within the micropores of the coal matrix, and adsorbed gas generally accounts for the dominant proportion of the total gas content in coal seams [8–10]. Therefore, under the complex conditions simulating deep formations, accurately evaluating the methane adsorption capacity of coal and its controlling mechanisms is fundamental to deep CBM resource assessment, reserve estimation, and optimization of development strategies. In deep coal seams, reservoir pressure often exceeds 15 MPa, and methane exists under high-pressure or even near-supercritical thermodynamic conditions. Its density, compressibility, and intermolecular interaction characteristics change significantly, causing coal-methane adsorption behavior to exhibit responses distinct from those observed under low-pressure conditions.

Deep high-pressure or near-supercritical conditions alone cannot independently determine methane adsorption behavior; rather, their influence on adsorption characteristics is highly dependent on the intrinsic structural properties of the coal matrix. Coal rank, as an integrated indicator of coalification evolution, is a key factor controlling methane adsorption capacity in coal reservoirs [11–13]. With increasing coal rank, the structural characteristics of coal macromolecules undergo pronounced differentiation: oxygen-containing functional groups (e.g., carboxyl and hydroxyl groups) are progressively eliminated [14,15], aliphatic side chains are shortened and cleaved [16,17], and condensed aromatic ring structures continuously expand and tend toward ordered stacking [18,19]. These evolutionary processes transform the coal molecular framework from a relatively flexible structure to a highly rigid configuration, thereby not only restructuring the pore system of the coal matrix but also profoundly influencing the intermolecular interactions between coal and methane molecules.

From the perspective of molecular-scale interaction mechanisms, an increase in the size of aromatic lamellae and their stacking density enhances the superposition effect of van der Waals potential energy between pore walls, thereby generating deeper potential wells and providing higher-energy adsorption sites [20–22]. Under high-pressure or near-supercritical conditions, the density of methane molecules increases significantly, and both intermolecular interactions and molecule-pore wall interactions are further amplified, making the influence of coal macromolecular structural differences on adsorption behavior more pronounced [23,24]. Therefore, the variations observed among different coal ranks in terms of methane adsorption capacity, adsorption heat characteristics, and pressure sensitivity can essentially be attributed to systematic differences in the chemical composition and spatial geometric configurations of coal macromolecules.

However, due to the pronounced heterogeneity and multiscale complexity of coal structures, conventional experimental techniques have difficulty directly elucidating adsorption mechanisms at the molecular scale under deep high-pressure conditions. In recent years, X-ray diffraction (XRD), Fourier transform infrared spectroscopy (FTIR), X-ray photoelectron spectroscopy (XPS), Solid-state ^{13}C nuclear magnetic resonance (^{13}C NMR), and high-resolution transmission electron microscopy (HRTEM) have been widely applied in studies of coal macromolecular structures, providing important experimental constraints for quantitatively characterizing functional group distributions, aromaticity, and microstructural ordering parameters of coal [25–31]. FTIR can qualitatively and semi-quantitatively analyze organic functional groups such as aliphatic, aromatic, and oxygen-containing groups; XPS accurately identifies the chemical states of C, O, N, and S heteroatoms on

the coal surface; 13C NMR quantitatively characterizes the aromatic carbon, aliphatic carbon, and carbon skeleton structure, which can fully provide the core parameters for coal macromolecular model construction. In contrast, XRD is effective for analyzing the physical stacking parameters of microcrystallites; it provides limited information on specific chemical connectivity. On this basis, molecular simulation methods have gradually become important tools for investigating coal-methane interactions. Previous studies have shown that coal macromolecular models constructed under experimental data constraints can effectively compensate for the limitations of experimental approaches in terms of spatial scale and operating conditions. For example, Firouzi et al. employed the Voronoi method to construct porous carbon network structures to simulate gas adsorption behavior in microporous media [32]. In contrast, Liu et al. established coal macromolecular models through geometric optimization and successfully predicted the adsorption characteristics of different gases [33]. These studies provide an important methodological foundation for elucidating coalbed methane adsorption mechanisms at the molecular scale. Nevertheless, existing research has primarily focused on single coal ranks or low-to-moderate pressure conditions, and the understanding of high-pressure or even near-supercritical methane adsorption behavior in deep coal seams remains insufficient. Meanwhile, systematic comparative investigations across multiple coal ranks are relatively scarce, making it difficult to reveal the continuous control pattern of coal macromolecular structural evolution on adsorption mechanisms.

In view of this, three representative coal samples of different ranks are selected in this study. The coal macromolecular structures are comprehensively characterized using FTIR, XPS, and ^{13}C NMR, and macromolecular models of different coal ranks are constructed under experimental constraints. Methane adsorption behavior under deep reservoir conditions is then systematically simulated. By comparing differences among models of various coal ranks in terms of molecular structural characteristics, pore structure evolution, methane adsorption capacity, and adsorption heat response, this study aims to elucidate the control mechanism of coal rank on high-pressure methane adsorption behavior in deep coal seams at the molecular scale, thereby providing a theoretical basis for the accurate evaluation and efficient development of deep CBM resources.

2. Samples and Experimental Methods

2.1. Basic Characteristics of Samples

Three coal samples with different metamorphic degrees were collected from the Qinshui Basin, Shanxi Province, China. The samples were obtained from the medium-rank Dongzhuang Mine (DZ), the high-rank Zhangcun Mine (ZC), and the high-rank Sihe Mine (SH). To ensure sample integrity, large blocks of freshly exposed coal were collected from newly exposed working faces and immediately sealed with multiple layers of plastic wrap to prevent oxidation and moisture loss.

According to ISO 7404-3-1994 and ISO 7404-5-1994 standards, the maximum vitrinite reflectance ($R_{o,max}$) was determined using polished particulate coal sections (particle size ~1.18 mm) [34,35]. Proximate analysis was conducted on crushed powder samples (particle size < 0.25 mm) in accordance with the Chinese National Standard GB/T 212-2008 to determine moisture (M_{ad}), ash yield (A_d), volatile matter (V_{daf}), and fixed carbon (F_{Cd}) [36]. Ultimate analysis (*C*, *H*, *N*, *S*) was performed following GB 476-1991 [37], and the oxygen content was calculated by difference. The detailed results are presented in Table 1. Notably, although the proximate and ultimate analysis results for DZ, ZC, and SH appear numerically similar, their fundamental differences are rooted in the progression of coal rank. DZ ($R_{o,max}$ = 1.63%) is a medium-rank coal with the highest volatile matter (V_{daf} =18.50%) and abundant aliphatic structures. ZC ($R_{o,max}$ = 2.29%) is a high-rank coal in the transitional

stage of coalification, with moderate volatile matter and enhanced aromatic condensation. SH ($R_{o,max}$ = 3.18%) is an anthracite with the lowest volatile matter (V_{daf} = 8.66%), the highest fixed carbon (FC_d = 77.41%), and the most aromatized structure. These obvious gradient differences provide a solid foundation for the comparison and construction of molecular models with different coal ranks.

Table 1. Results of Ultimate and Proximate Analyses of Coal Samples.

Sample Code	Ultimate Analysis/%					Proximate Analysis (%)				$R_{o,max}$ %
	C_{daf}	H_{daf}	O_{daf}	N_{daf}	$S_{t,d}$	M_{ad}	A_d	V_{daf}	F_{Cd}	
DZ	87.86	4.22	3.58	1.60	2.69	1.84	6.15	18.50	76.49	1.63
ZC	89.12	4.09	4.81	1.57	0.34	1.34	16.74	14.73	70.99	2.29
SH	91.25	2.71	4.35	1.35	0.29	3.70	15.24	8.66	77.41	3.18

2.2. Experimental Methods

To accurately characterize the macromolecular chemical structures of coal and construct representative coal macromolecular models, FTIR, ^{13}C NMR, and XPS were employed for combined analysis. All coal samples were ground into fine powders (particle size < 200 mesh) prior to testing to minimize particle size effects on the results. The samples were subsequently vacuum-dried at 378.15 K for 12 h to thoroughly remove free and adsorbed water, thereby avoiding interference from moisture in functional group identification and surface chemical state analysis.

(1) XPS

The surface elemental composition and chemical states of the coal samples were analyzed using XPS. During measurement, the beam spot size was 900 μm, and tests were conducted under standard ultra-high vacuum conditions (base pressure < 10^{-9} mbar to prevent signal attenuation). To improve the signal-to-noise ratio and measurement stability, 30 full-spectrum scans were performed for each sample to obtain elemental composition information. As coal is a non-conductive material, surface charging effects inevitably occurred during testing. To eliminate charging-induced shifts in binding energy determination, all spectra were calibrated using the main C1s peak at 284.8 eV as the reference, providing a strict binding energy measurement accuracy of ±0.1 eV. High-resolution scans and peak deconvolution of characteristic peaks such as C1s and O1s were conducted to semi-quantitatively determine the relative contents of different chemical bond types (e.g., C–C/C=C, C–O, C=O, and O–C=O), thereby providing constraint parameters for functional group construction in the coal macromolecular models.

(2) FTIR

The organic functional group structures in the coal samples were characterized using FTIR with a Bruker Vertex 80 spectrometer, Karlsruhe, Germany. Samples were prepared using the KBr pellet method, in which coal powder was uniformly mixed with KBr at a specified mass ratio and pressed under 20 MPa for 60 s to form transparent pellets. Spectra were recorded over a wavenumber range of 4000–400 cm^{-1} with a resolution of 4 cm^{-1}. This high spectral resolution ensures the precise identification of adjacent absorption bands. Each sample was scanned 32 times to improve the signal-to-noise ratio and minimize background interference. By analyzing absorption peak distributions in different wavenumber regions, aliphatic C–H, aromatic C=C, and oxygen-containing functional groups (e.g., hydroxyl, carboxyl, and ether groups) were qualitatively and semi-quantitatively identified, providing experimental evidence for the types and relative abundances of functional groups in the coal macromolecules.

(3) Solid-state ^{13}C NMR

The carbon skeleton structures of the coal samples were analyzed using a Bruker Avance III 600 MHz solid-state ^{13}C NMR spectrometer, Karlsruhe, Germany, which provides exceptionally high magnetic field stability and chemical shift resolution. Measurements were conducted with a 4 mm magic-angle spinning (MAS) probe at a spinning rate of 10 kHz to effectively average anisotropic interactions and enhance spectral resolution. Cross-polarization/magic-angle spinning (CP/MAS) was employed with a contact time of 2 ms and a recycle delay of 3 s to balance signal intensity and experimental efficiency. Signals in different chemical shift regions were analyzed to distinguish aromatic carbon, aliphatic carbon, and oxygenated carbon species, and their relative proportions were calculated to quantitatively constrain aromaticity and carbon structure distribution in the coal macromolecular models.

(4) Spectral deconvolution and semi-quantitative analysis

To accurately identify and quantitatively characterize the chemical structural features of the coal samples, peak deconvolution was performed on FTIR, XPS, and ^{13}C NMR spectra using PeakFit 4.1.2 software. During fitting, peak positions were reasonably constrained based on the published literature and standard spectral databases, and peak shape parameters were optimized using the least-squares method to ensure the physical and chemical reliability of the results. The integrated areas of characteristic peaks were used for semi-quantitative calculation of the relative abundances of different elements, chemical bonds, or functional groups [31]. These results served as essential input parameters for coal macromolecular model construction, constraining functional group composition, aromatic/aliphatic carbon ratios, and overall chemical structural characteristics.

3. Results and Molecular Model Construction

3.1. Structural Characterization of Coal Samples

3.1.1. Functional Group Distribution by FTIR

The FTIR spectra were divided into four main absorption regions based on standard corresponding functional groups: the hydroxyl (-OH) region (3200–3600 cm^{-1}), the aliphatic C-H stretching and bending regions (2800–3000 cm^{-1} and 1350–1450 cm^{-1}), the oxygen-containing and aromatic C=C ring stretching region (1000–1800 cm^{-1}), and the aromatic C-H out-of-plane deformation region (700–900 cm^{-1}). As the coal rank increases from DZ ($R_{o,max}$ = 1.63%) to SH ($R_{o,max}$ = 3.18%), the overall FTIR spectral profiles of the three samples are generally similar; however, the relative intensities of characteristic absorption bands exhibit systematic variations with increasing coalification (Figure 1). In the hydroxyl region (3200~3600 cm^{-1}), all samples display a broad absorption band attributed to hydrogen-bonded -OH groups. The intensity of this band gradually decreases with increasing coal rank, reflecting progressive deoxygenation and the consequent reduction in hydrophilicity. In the aliphatic region (2800~3000 cm^{-1} and 1350~1450 cm^{-1}), the medium-rank DZ sample shows the sharpest and most intense aliphatic absorption peaks. As the coal rank increases to ZC and SH, these peaks weaken markedly and nearly disappear in the SH sample. This observation indicates that, during the advanced stage of coalification, substantial cleavage and elimination of aliphatic side chains and bridging bonds occur within the macromolecular network. In contrast, in the aromatic region (700~900 cm^{-1}), the out-of-plane C-H bending vibrations of aromatic rings become more distinct and structurally complex in the SH sample. This evolutionary trend suggests that, with increasing coalification, aliphatic substituents are progressively removed, followed by directional rearrangement and cross-condensation of aromatic rings, leading to an increased degree of aromatic condensation. Consequently, the coal macromolecular structure

gradually evolves toward a more ordered, graphite-like layered configuration. Overall, the structural evolution is characterized by a progressive loss of aliphatic structures and enhanced aromatic condensation.

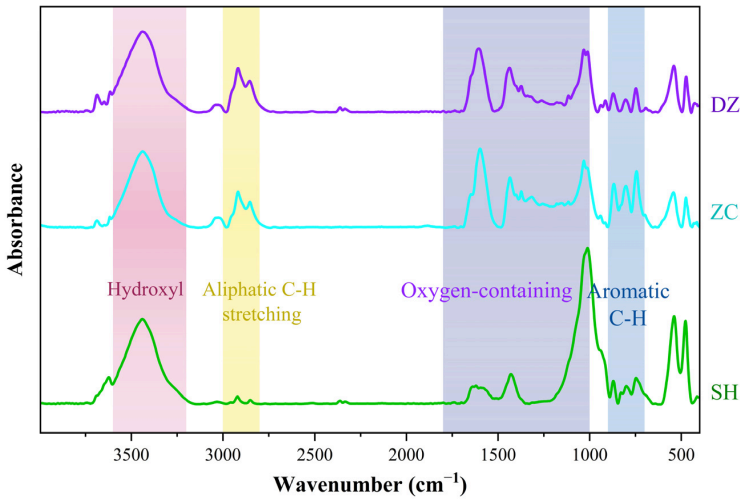


Figure 1. Evolution characteristics of FTIR spectra.

3.1.2. Heteroatom Speciation by XPS

The N1s and S2p spectra were deconvoluted using PeakFit software, and the chemical states of the elements in coal were identified according to their characteristic binding energies. The fitting results are shown in Figure 2. Nitrogen in coal predominantly exists as pyrrolic nitrogen (N-6), followed by quaternary/graphitic nitrogen (N-Q), whereas pyridinic nitrogen (N-5) accounts for the lowest proportion. With increasing coal rank, the relative content of quaternary/graphitic nitrogen increases significantly, while the proportions of pyrrolic and pyridinic nitrogen gradually decrease. This indicates that during progressive coalification, nitrogen-containing heterocyclic structures undergo condensation and structural transformation toward thermodynamically more stable graphitic lattice configurations.

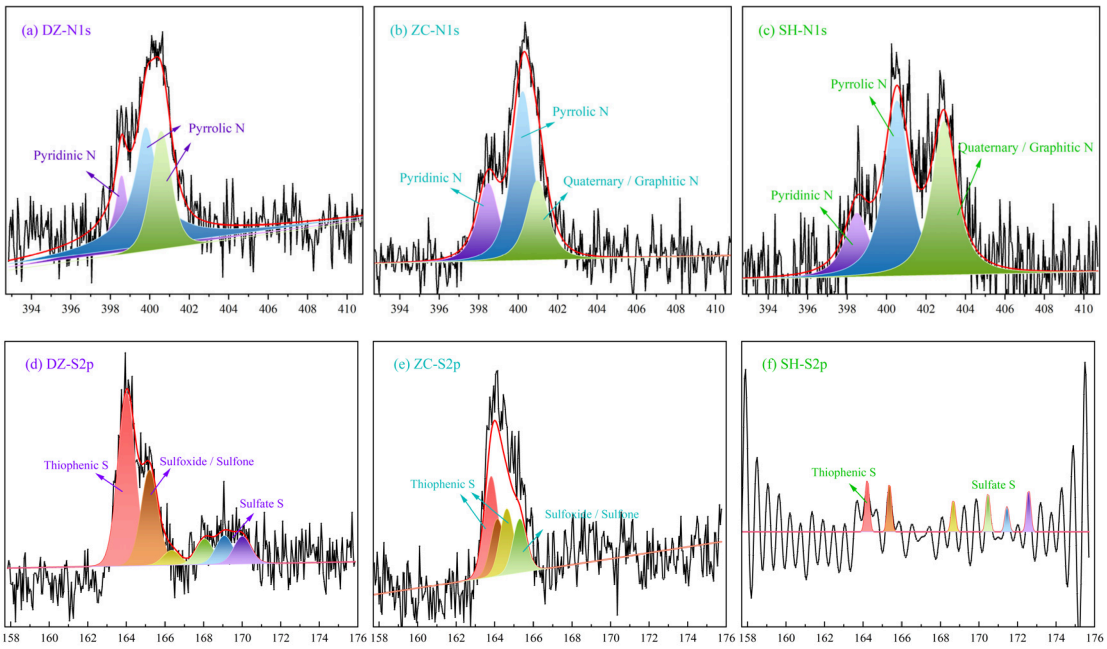


Figure 2. Deconvoluted N1s and S2p XPS spectra of coal samples with different coal ranks.

Sulfur in coal mainly exists as thiophenic sulfur. As coal rank increases, the relative content of thiophenic sulfur shows a pronounced upward trend, whereas the proportions of sulfoxide and sulfone sulfur continuously decrease. Meanwhile, as shown in Table 1, the total sulfur content of the SH sample is only 0.29%. The substantial reduction in sulfur content leads to extremely high spectral noise.

3.1.3. Carbon Skeleton Analysis by ^{13}C NMR

^{13}C NMR spectroscopy is a key technique for quantitatively characterizing the carbon skeletal structure of coal macromolecules. According to chemical shift assignments, the spectra can be divided into three major structural regions: the aliphatic carbon region (0–95 ppm), the aromatic carbon region (95–165 ppm), and the carbonyl/carboxyl carbon region (>165 ppm). A comparison of the spectral characteristics at different coal ranks shows that, as coalification progresses from DZ ($R_{o,max}$ = 1.63%) to SH ($R_{o,max}$ = 3.18%), both the absolute intensity and relative area of the main aromatic carbon peak increase markedly, and the peak shape becomes progressively sharper and more symmetrical. This indicates that aromatic carbon constitutes the dominant component of the coal molecular structure, and that higher coal rank corresponds to a greater degree of structural ordering and aromatic condensation.

The ratio of bridge carbon to peripheral carbon (XBP) reflects the degree of condensation and structural complexity of aromatic rings in coal and can be used to estimate the size of aromatic clusters. The calculation is given in Equation (1):

$$X_{BP} = \frac{f_\alpha^B}{f_\alpha^H + f_\alpha^P + f_\alpha^S} \quad (1)$$

Note: f_α^H, protonated aromatic carbon; f_α^P, aromatic carbon bonded to hydroxyl or ether groups; f_α^S, aromatic carbon bonded to aliphatic chains; f_α^B, bridge carbon.

Based on the chemical shift assignments and relative peak areas in the ^{13}C NMR spectra (Figure 3), the structural parameters of coal macromolecules were calculated. The XBP values of the DZ, ZC, and SH samples are 0.34, 0.39, and 0.48, respectively. With increasing coal rank, pronounced aromatic condensation occurs within the macromolecular skeleton. The aromatic clusters gradually evolve from relatively small ring systems containing 2–3 rings to larger polycyclic aromatic systems composed of multiple fused benzene rings, and the macromolecular framework becomes progressively more stable. Detailed peak-fitting parameters for XPS and ^{13}C NMR spectra, including peak positions, assignments, and relative integrated areas, are provided in the Supplementary Information (Tables S1 and S2).

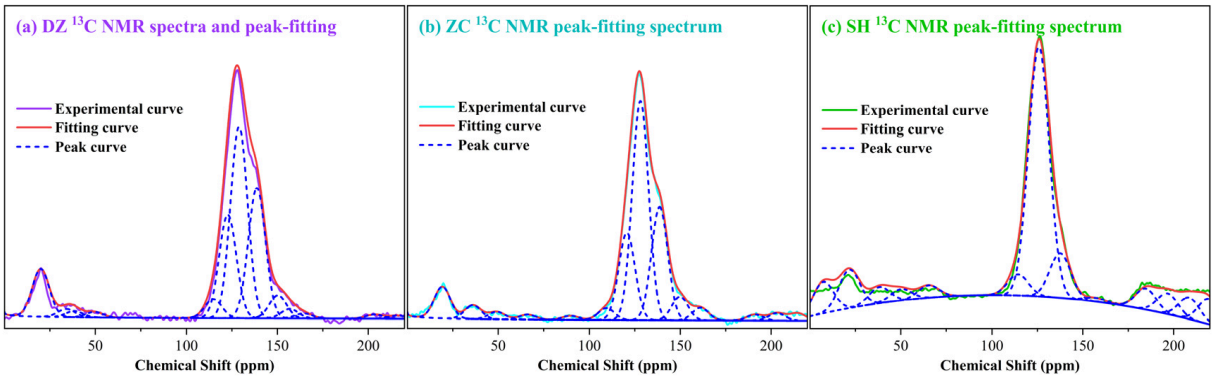


Figure 3. Experimental ^{13}C NMR spectra and peak-fitting results of coal samples with different coal ranks.

3.2. Molecular Model Construction

3.2.1. Two-Dimensional Molecular Structure

Based on the key structural parameters obtained from FTIR, XPS, and ^{13}C NMR, the initial 2D molecular skeletons of the DZ, ZC, and SH coal samples were constructed in this section. To ensure model accuracy, the planar macromolecular structures of coal samples with different ranks were constructed using ChemSketch 2024.2.3 software, and the corresponding chemical shifts were calculated. A construction-calculation-correction strategy was adopted to iteratively optimize and validate the models. As shown in Figure 4, the theoretical ^{13}C NMR spectra of the 2D structures were simulated using the ACD/CNMR Predictor algorithm. By repeatedly adjusting the number of aromatic cores, bridging structures, and side-chain lengths, the final chemical shift characteristics of the three 2D molecular models were determined. The molecular structural evolution illustrated in Figure 4 shows that, with increasing coal rank, aliphatic side chains and bridging bonds in the coal macromolecules decrease substantially, heteroatom-containing functional groups are progressively eliminated, and the size of the condensed aromatic ring systems increases markedly. Specifically, the medium-rank DZ model retains a relatively open framework with abundant oxygen-containing functional groups and longer aliphatic side branches. In contrast, the ZC model exhibits an intermediate state of partial condensation, while the high-rank SH model is dominated by compact, large polycyclic aromatic hydrocarbons with minimal peripheral appendages. As the metamorphic grade reaches the SH stage, the chemical evolution is dominated by dehydrogenation and the cross-linking condensation of aromatic rings, driving the gradual evolution of the macromolecular structure toward a more ordered, graphite-like layered configuration. The good agreement between the calculated and experimental spectra confirms that the constructed 2D models realistically represent the microscopic chemical structures of coal samples at different ranks.

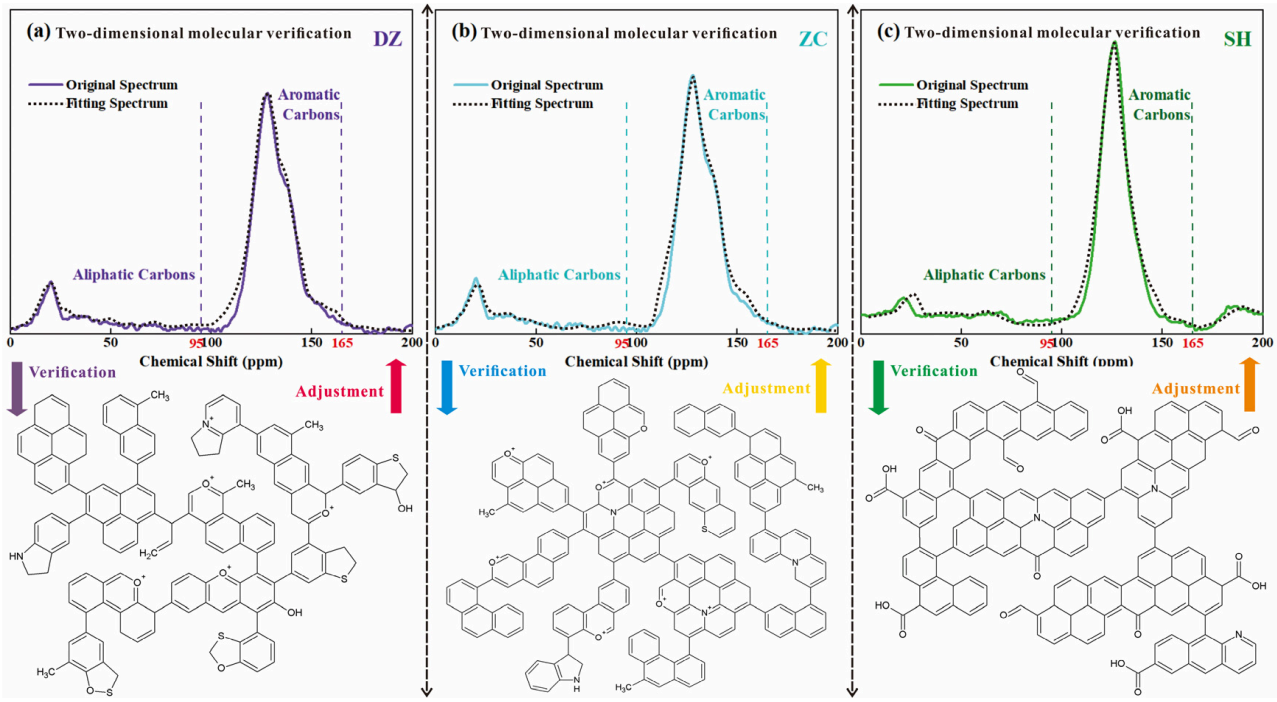


Figure 4. Comparison between calculated and experimental spectra and the 2D macromolecular models of coal.

3.2.2. Three-Dimensional Unit Cell Parameters

To realistically reproduce the microscopic occurrence environment of deep coal reservoirs, 3D aggregate models were constructed based on the previously established 2D skeletons. The unit cell models of coal samples with different ranks are shown in Figure 5. Using the COMPASS III force field, the coal molecules were subjected to geometry optimization, annealing, and dynamic optimization in the Forcite module to obtain 3D macromolecular structure models. The molecular formulas are $C_{144}H_{105}N_2O_8S_4$ for DZ, $C_{200}H_{125}N_4O_7S$ for ZC, and $C_{150}H_{83}N_3O_{17}$ for SH. The coal macromolecular unit cells were constructed using the Amorphous Cell (AC) module. The initial cell dimensions were set to 4.00 × 4.00 × 4.00 nm (a = b = c). According to the coal rank evolution trend, the target densities of DZ, ZC, and SH were set to 1.40, 1.50, and 1.60 g/cm^3, respectively. High-energy overlaps in the initial configurations were eliminated, and the structures were optimized to reach the global minimum energy state. Ultimately, 26 model molecules were added for DZ, resulting in a unit cell formula of $C_{3744}H_{2730}N_{52}O_{208}S_{104}$; 22 model molecules were added for ZC, yielding $C_{4400}H_{2750}N_{88}O_{154}S_{22}$; and 28 model molecules were added for SH, giving $C_{4200}H_{2324}N_{84}O_{476}$.

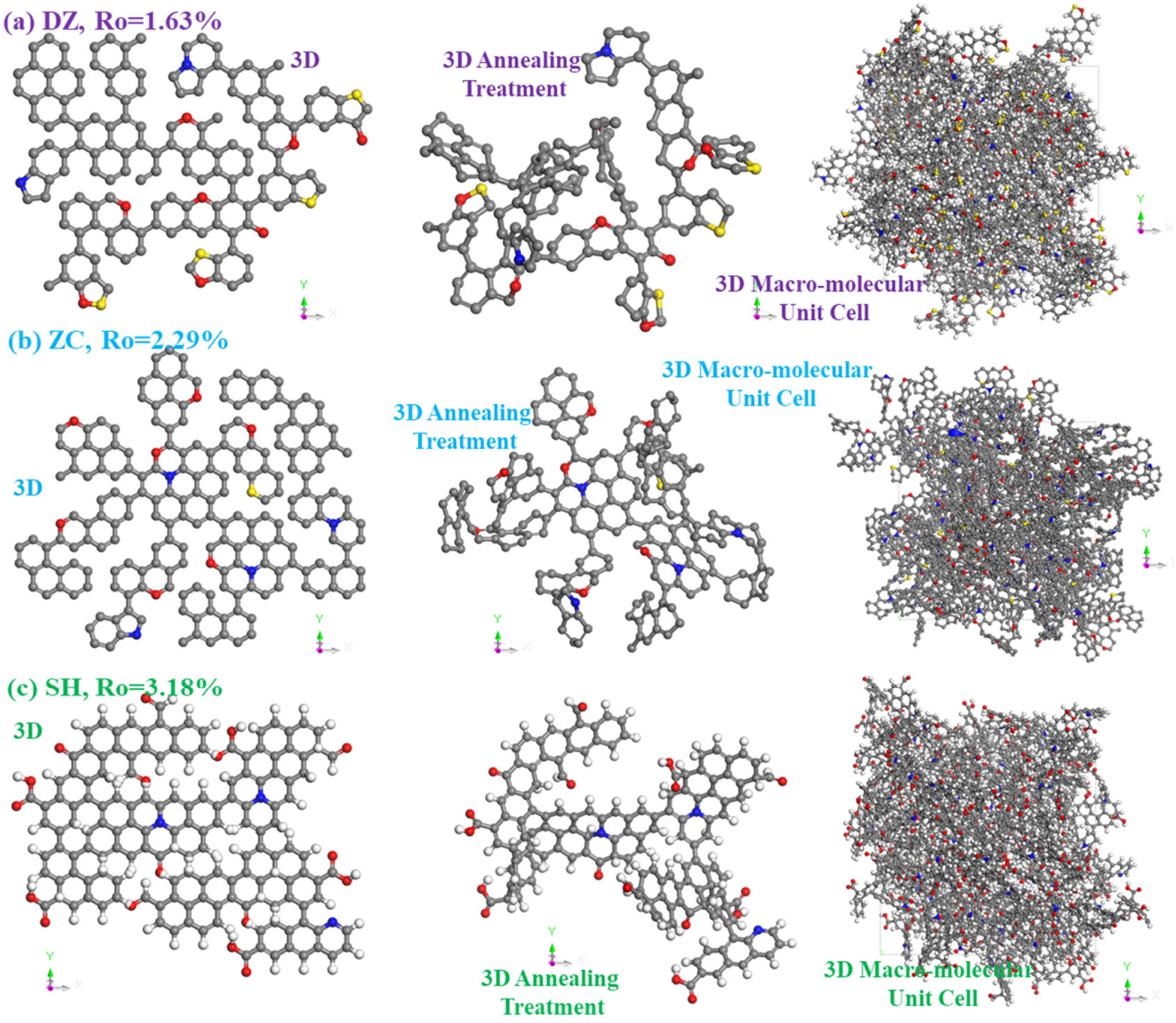


Figure 5. Construction of three-dimensional macromolecular model.

3.2.3. Coal Matrix Pore Model

To quantitatively characterize the microscopic pore evolution of coal macromolecular models with different ranks, the Atom Volumes and Surfaces tool in Materials Studio was employed. With a probe radius of 1.0 Å, the free volume (V*f*) and Connolly surface area of the models were calculated, representing the accessible space for gas accumulation and the effective interaction interface within the coal matrix, respectively. Micropores (pore diameter < 2 nm) dominate the pore structure of coal and serve as the primary sites for methane adsorption [3]. To simulate gas behavior under realistic conditions, intergranular slit pores were constructed using the Builder module, and the pore width was uniformly set to 2 nm for all coal samples. This configuration was designed to compare the differences in gas–solid interactions on coal surfaces of different ranks under identical spatial confinement conditions. It should be noted that this 2 nm slit model serves solely as a controlled probe to visualize localized adsorption affinity and density distributions; the quantitative conclusions regarding macroscopic adsorption capacity and the rank-dependent trend are derived exclusively from the slit-free bulk matrix models.

3.2.4. Adsorption Parameter Settings

Methane adsorption simulations were performed using the GCMC method in the Sorption module with the Adsorption Isotherm task. The Metropolis algorithm was applied, the COMPASS III force field was selected, and the calculation accuracy was set to Ultra-fine. To simulate deep coal reservoir conditions, the temperature was set to 313.15 K, and the pressure ranged from 10 to 20,000 kPa, with 10 adsorption points defined. Electrostatic interactions and van der Waals interactions were calculated using the Ewald summation and atom-based summation methods, respectively. The adsorbent was the previously constructed coal matrix pore-micropore model, and the adsorbate was CH_4, whose molecular structure was geometrically optimized prior to simulation.

4. Discussion

4.1. Comparative Analysis of Pore Structure in the Models

As shown in Figure 6, from the medium-rank coal DZ (*Ro* = 1.63%) to the anthracite SH (*Ro* = 3.18%), V*f* decreases significantly from 5108.39 Å^3 to 3999.87 Å^3, indicating a pronounced decline in free volume with increasing coal rank. This trend confirms that the continuous growth and oriented stacking of aromatic layers during coalification produce a densification effect, physically compressing the primary pores within the coal matrix and resulting in a gradual reduction in total pore space.

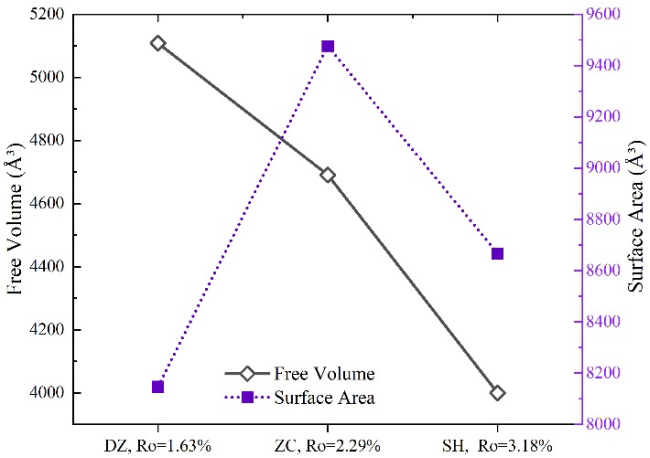


Figure 6. Evolution of V*f* and Connolly surface area of coal macromolecules with increasing coal rank.

Notably, the pore surface area does not decrease synchronously with pore volume but instead exhibits a trend of initial increase followed by a decline. The high-rank coal ZC (Ro = 2.29%) exhibits the largest internal surface area of 9476.65 Å^2, exceeding that of DZ (8147.13 Å^2) and SH (8666.67 Å^2). This phenomenon suggests that during the transitional ZC stage, the extensive cleavage of aliphatic side chains and the partial, irregular condensation of aromatic rings create a highly fragmented and rough micro-pore network. This structural roughening maximizes the specific surface area available for gas adsorption, even as the total pore volume contracts. However, as coal rank further evolves to the anthracite stage (the SH sample), the structural evolution is dominated by the highly ordered alignment and parallel stacking of large polycyclic aromatic hydrocarbons (the tendency of graphitization). This extreme structural densification not only induces micropore collapse but also significantly smooths the internal pore walls, ultimately resulting in the simultaneous reduction in both volume and surface area.

Figure 7 visualizes this three-dimensional morphological pattern, where the blue regions represent methane-accessible free volume (pores) and the gray regions represent the Connolly surface area of the coal matrix. In DZ (Figure 7a), the pore network is characterized by large and well-connected channels; in contrast, SH (Figure 7c) exhibits a highly fragmented pore topology. For the anthracite SH, excessive structural densification leads to pore collapse, accompanied by decreases in both free volume and surface area. This morphological transition from a connected network to a fragmented structure confirms that high-rank coal possesses a denser and more closed matrix structure.

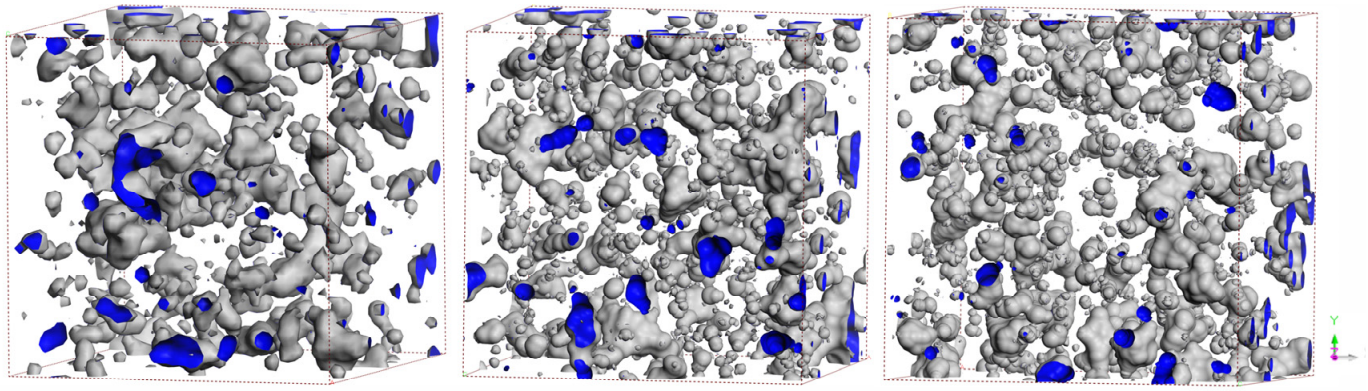


Figure 7. Spatial distribution of internal free volume (blue regions) in coal matrix models with different coal ranks.

4.2. Evolution of High-Pressure Methane Adsorption Performance

This section focuses on the adsorption behavior of methane in coal matrix models with different ranks. The average number of methane molecules loaded in the three coal samples at different pressures obtained from the original simulations is shown in Figure 8a. Within the pressure range of 0.001–20 MPa, the number of loaded molecules in all samples increases with pressure, and the growth gradually levels off after 16 MPa. At the saturation pressure of 20 MPa, the microscopic loading follows the trend ZC > SH > DZ, with ZC exhibiting the highest molecular loading (484.50 molecules/cell). This phenomenon indicates that, within simulation systems of identical volume, higher-rank coals (ZC and SH) exhibit stronger methane adsorption capacity due to their relatively denser skeletal structures.

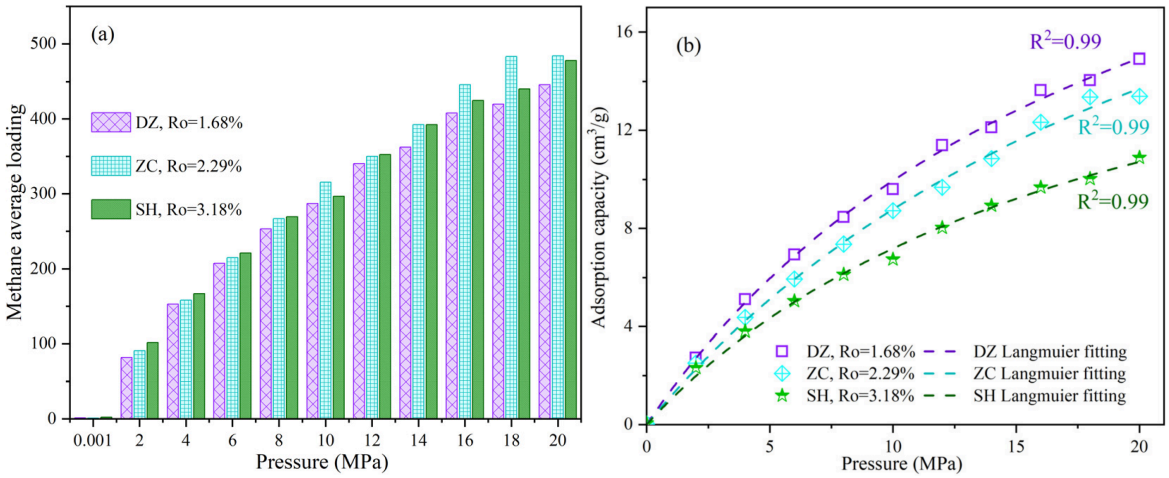


Figure 8. Adsorption capacity of different coal ranks. (**a**) Number of methane molecules loaded. (**b**) Corrected high-pressure adsorption isotherms.

To further evaluate the intrinsic adsorption performance of the coal matrix, the simulated microscopic loading must be converted into macroscopic adsorption capacity. It should be noted that the simulated output parameter, N_{Load}, represents the total number of adsorbed methane molecules within a single unit cell at thermodynamic equilibrium, including those located in both the skeletal framework and the slit pore space. To eliminate the counting interference caused by methane adsorption in the slit pore space and to more accurately reflect the adsorption capacity per unit mass of coal, Equation (2) was incorporated, and an effective free-volume ratio (V_{Ratio}) was introduced to correct the adsorption amount (Equation (2)). The corrected high-pressure adsorption isotherms are shown in Figure 8b. For all samples, the methane adsorption capacity increases with pressure and approaches saturation near 20 MPa. The corrected macroscopic adsorption capacity exhibits a trend distinctly different from that of the original loading numbers: DZ > ZC > SH. At 20 MPa, the adsorption capacities of DZ, ZC, and SH are 14.91, 13.39, and 10.89 cm^3/g, respectively.

$$V_{ad} = \frac{N_{Load} \times V_m}{N_A \times M_{cell}} \times 10^3 \times V_{Ratio} \quad (2)$$

Note: V_{ad} is the adsorption capacity, cm^3/g; N_{Load} is the number of adsorbed molecules within a single unit cell; V_m is the molar volume of an ideal gas at standard conditions, 22.414 L/mol; N_A is Avogadro's constant, 6.02 × 10^{23} mol^{-1}; M_{cell} is the mass of the unit cell, g/cell; V_{Ratio} is the ratio of the free volume within the unit cell to the total unit cell volume.

Figure 9a clearly illustrates the discrepancy between microscopic loading and macroscopic adsorption capacity, which fundamentally arises from the compressive effect of coal rank evolution on the available adsorption space. On the one hand, as the vitrinite reflectance increases from 1.63% to 3.18%, the densification degree of the coal macromolecular framework increases significantly, with the density rising from 1.47 g/cm^3 to 1.60 g/cm^3. This densification process directly compresses the intrinsic pore space within the coal matrix, resulting in a decrease in the effective free-volume ratio from 8.23% for DZ to 6.26% for SH. On the other hand, although the high-rank coal ZC possesses the largest specific surface area (see Section 4.1), its corrected macroscopic adsorption capacity is lower than that of DZ. This phenomenon indicates that under the high-pressure condition of 20 MPa, methane occurrence in coal micropores no longer strictly follows a surface-area-dominated monolayer adsorption mechanism, but instead shifts to a pore-volume-controlled micropore filling

mechanism. Under these conditions, methane molecules confined within the pores exhibit high-density quasi-liquid behavior, causing the effective *Vf* to replace specific surface area as the primary factor controlling the upper adsorption limit. Although the DZ sample has a slightly lower surface area, its looser framework and more abundant effective adsorption space (Figure 9a) enable it to achieve the highest mass-based adsorption percentage despite a lower molecular loading number. These results demonstrate that, in the dry basis model, effective free volume is the dominant factor governing macroscopic adsorption capacity.

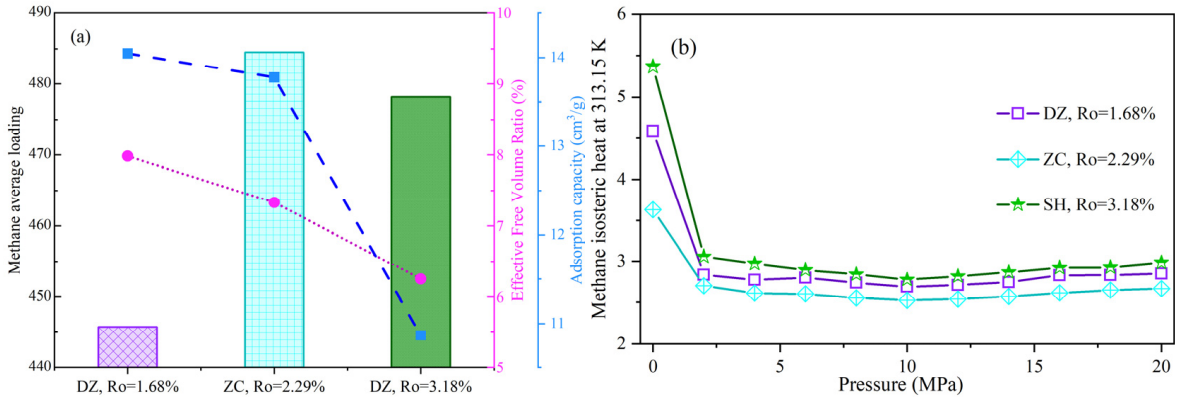


Figure 9. Adsorption characteristics of different coal ranks. (**a**) Correlation between effective free-volume ratio and adsorption capacity. (**b**) Variation in methane isosteric heat of adsorption with pressure at 313.15 K.

Figure 9b calculates the isosteric heat of adsorption under different pressures. For all samples, the adsorption heat stabilizes within 2.6–3.0 kcal/mol in the high-pressure region, confirming that methane adsorption on the coal matrix is physical adsorption dominated by van der Waals interactions. The anthracite SH exhibits the highest adsorption heat, indicating the strongest energetic attraction between its pore surfaces and methane molecules. However, this stronger interaction energy does not compensate for the loss of free volume caused by matrix densification. To further quantify the trade-off between enhanced adsorption potential and reduced storage space, a simple adsorption capacity index can be defined as the product of the average isosteric heat of adsorption and the effective free volume fraction. Take the isosteric heat of adsorption at 20 MPa for DZ, ZC, and SH, which are 2.85, 2.67, and 2.90 kcal/mol, respectively (Figure 9b); and multiplying by the corresponding effective free volume fractions (7.78%, ~7.33%, and 6.25%); the resulting indices are 22.21 (DZ), 19.56 (ZC), and 18.14 (SH), which is completely consistent with the macroscopic adsorption capacity order of DZ > ZC > SH. The quantitative trade-off calculation directly proves that the loss of effective free volume caused by coal matrix densification outweighs the enhancement of adsorption potential energy, which is the fundamental reason for the lowest adsorption capacity of SH with the highest adsorption heat. Therefore, methane occurrence in coal results from the combined effects of energetic attraction and spatial confinement. With increasing coal rank, matrix densification substantially reduces the effective storage space; even though the adsorption potential is enhanced, the macroscopic adsorption capacity still exhibits a decreasing trend.

Furthermore, it is also pertinent to consider the potential influence of reservoir temperature on the conclusions drawn from the simulations performed at 313.15 K. Deep coal reservoirs frequently exhibit temperatures in the range of 333–373 K, and adsorption is an exothermic process; consequently, absolute methane adsorption capacities are expected to decrease with increasing temperature due to enhanced molecular kinetic energy and reduced gas–solid affinity. However, the fundamental transition from surface-area-dominated to volume-dominated adsorption behavior is unlikely to be reversed, and may even be

accentuated, at elevated temperatures. At higher thermal energy, methane molecules are less readily trapped in localized surface potential wells, thereby further diminishing the relative contribution of specific surface area to the total storage capacity. In contrast, the accessible free volume represents a rigid, temperature-independent geometric constraint of the coal matrix that dictates the maximum number of molecules that can be accommodated under high-pressure, supercritical-like conditions. Since the effective free volume fraction is an intrinsic structural property governed by coal rank and the degree of aromatic layer stacking, even under high-temperature deep reservoir conditions, the medium-rank coal (DZ) with its looser framework will retain a superior maximum adsorption capacity compared to the severely densified anthracite (SH).

4.3. High-Pressure Methane Adsorption Mechanism at Different Coal Ranks

By comparing differences in pore evolution, adsorption performance, and thermodynamic properties among coal rank models, the microscopic mechanism governing deep coalbed methane occurrence can be clarified: the control of coal rank on methane adsorption is essentially constrained by both adsorption space and potential energy strength. With increasing coal rank, the adsorption mechanism evolves from volume-filling dominance to surface potential-controlled behavior. As shown in Figure 10, when the pressure increases from 0.001 MPa to 20 MPa, methane molecules (red) within each coal sample transition from sparse adsorption to high-density filling, exhibiting distinctly different spatial distribution characteristics under high-pressure conditions.

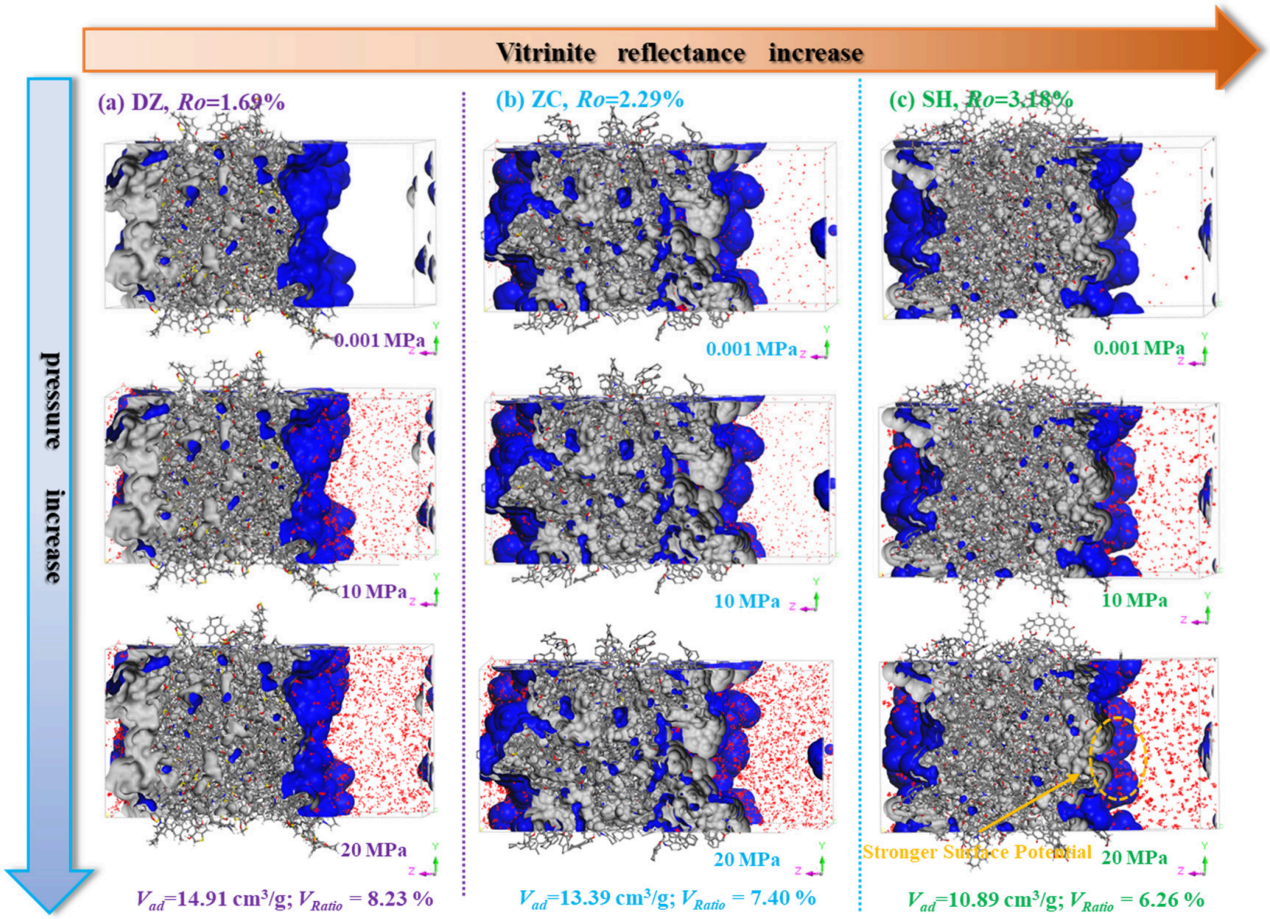


Figure 10. Comparison of the microscopic occurrence states of methane molecules (red) in coal matrices of different ranks under varying pressures. (Blue represents the pore surface, and red denotes adsorbed methane.).

In the medium-rank DZ model (Figure 10a), methane molecules display a typical volume-filling distribution pattern. The coal matrix framework is relatively loose, and the spacious, interconnected pore network provides abundant accessible free volume for methane. Methane molecules are uniformly and loosely distributed within the central regions of the wide pore channels, without exhibiting strong adhesion to the pore walls. This confirms that the relatively shallow potential wells in medium-rank coal primarily constrain methane molecules by the capacity of the adsorption space rather than by surface forces. In contrast, in the high-rank anthracite SH model (Figure 10c), methane molecules clearly exhibit a pronounced wall-adhering effect. Although the effective pore space is extremely narrow, the red methane molecules are tightly confined near the blue pore surfaces, forming locally high-density adsorption layers and significantly increasing CH_4 adsorption intensity per unit volume. This observation is highly consistent with the thermodynamic calculations, indicating that the highly oriented stacking of aromatic lamellae in anthracite forms deep van der Waals potential wells, generating strong adsorption affinity for methane and forcing gas molecules to pack into microscopic folds and slits at higher densities under high pressure.

In summary, the high-density adsorption of methane molecules on the pore surfaces of high-rank coal confirms their strong adsorption affinity for methane. The increased degree of aromatization enhances the surface potential energy, thereby increasing the local adsorption density of methane from a chemical perspective. However, the overall decrease in methane adsorption capacity from DZ to SH indicates that the dense pore volume of deep coal reservoirs physically compresses the effective storage space for methane, thereby constraining the upper limit of adsorption capacity. Although high-rank coal theoretically has the thermodynamic potential to capture high-density methane, this advantage is constrained by the extremely low utilization efficiency of its effective free volume, significantly limiting the methane storage performance of high-rank coal reservoirs. This study elucidates the high-pressure methane adsorption characteristics of coal reservoirs with different ranks, effectively correcting the application bias of traditional adsorption models under deep conditions, and provides a critical theoretical basis for the accurate evaluation of deep coalbed methane in complex occurrence environments.

5. Conclusions

Based on the combined characterization of FTIR, XPS, and ^{13}C NMR, this study reveals the evolution of the chemical structure and skeletal characteristics of coal macromolecules during coal rank progression. Under experimental constraints, macromolecular models of coals with different ranks were constructed, and the methane adsorption behavior and its controlling mechanisms under deep, high-pressure conditions were further elucidated at the molecular scale. The main conclusions are as follows:

(1) As the coal rank increases from 1.63% to 3.18%, the free volume decreases from 5108.39 $Å^3$ to 3999.87 $Å^3$, while the effective free-volume ratio declines from 8.23% to 6.26%, resulting in a reduction in macroscopic adsorption capacity. At the molecular scale, the coal matrix exhibits a pronounced densification trend, and its control over deep, high-pressure methane adsorption primarily manifests through compression of the effective free volume.

(2) At 20 MPa, the microscopic loading of methane within the unit cell follows the order ZC > SH > DZ, indicating that higher-rank coal pore surfaces possess stronger local adsorption capacity for methane. However, after correction using the free-volume ratio, the macroscopic adsorption capacity exhibits the opposite trend (DZ > ZC > SH), demonstrating that, under deep, high-pressure conditions, specific surface area or

local potential energy strength alone is insufficient to accurately predict the actual gas storage capacity of coal.

(3) As the pressure increases in the deep reservoir range, the occurrence state of methane in coal micropores gradually shifts from surface adsorption at low pressure to high-density quasi-liquid filling behavior. The adsorption isotherms of all coal samples tend to approach saturation within this pressure interval. Under high-pressure conditions, specific surface area is no longer the dominant parameter controlling adsorption behavior; instead, effective free volume becomes the key factor determining the upper adsorption limit.

(4) The control of coal rank on deep high-pressure methane adsorption is essentially characterized by the competitive interplay between enhanced potential energy and spatial confinement. The isosteric heat of adsorption for anthracite SH stabilizes at 2.6–3.0 kcal/mol, indicating that its aromatic lamellae construct deeper van der Waals potential wells and provide stronger local adsorption capacity. However, the insufficient free volume caused by excessive densification significantly weakens this potential advantage, thereby limiting its overall adsorption capacity.

Supplementary Materials: The following supporting information can be downloaded at: https://www.mdpi.com/article/10.3390/pr14091409/s1, Table S1: XPS peak fitting parameters for N1s and S2p spectra; Table S2: ^{13}C NMR chemical shift assignments and relative integrated areas.

Author Contributions: Conceptualization, W.N., M.H., T.Z. and M.C.; Methodology, W.N. and M.H.; Resources, M.C.; Data curation, W.N., M.H. and T.Z.; Writing—original draft, W.N., M.H., T.Z. and M.C.; Writing—review & editing, W.N., M.H., T.Z. and M.C.; Supervision, M.C.; Funding acquisition, M.C. All authors have read and agreed to the published version of the manuscript.

Funding: This work is supported by the Science and Technology Program of Xinjiang Uyghur Autonomous Region (2025B01009-2), the Key Research and Development Program of Xinjiang Uygur Autonomous Region (2024B01017-2) and the Youth Science Foundation of the Natural Science Foundation of Xinjiang Uygur Autonomous Region (Grant No. 2025D01C256).

Data Availability Statement: The original contributions presented in this study are included in the article/Supplementary Materials. Further inquiries can be directed to the corresponding author.

Acknowledgments: Sincere thanks are given to the Editors and Reviewers for their careful comments on the manuscript, which greatly improved the quality of the paper.

Conflicts of Interest: The authors declare no conflict of interest.

References

1. Karacan, C.Ö.; Field, R.A.; Olczak, M.; Kasprzak, M.; Ruiz, F.A.; Schwietzke, S. Mitigating climate change by abating coal mine methane: A critical review of status and opportunities. *Int. J. Coal Geol.* **2024**, *295*, 104623. [CrossRef]
2. Moore, T.A. Coalbed methane: A review. *Int. J. Coal Geol.* **2012**, *101*, 36–81. [CrossRef]
3. Zhu, Q.; Du, X.; Zhang, T.; Yu, H.; Liu, X. Investigation into the variation characteristics and influencing factors of coalbed methane gas content in deep coal seams. *Sci. Rep.* **2024**, *14*, 18813. [CrossRef]
4. Flores, R.M.; Moore, T. Coalbed gas: A review of research directions from the past to the future as facilitated by bibliometrics. *Int. J. Coal Geol.* **2025**, *298*, 104683. [CrossRef]
5. Li, S.; Qin, Y.; Tang, D.; Shen, J.; Wang, J.; Chen, S. A comprehensive review of deep coalbed methane and recent developments in China. *Int. J. Coal Geol.* **2023**, *279*, 104369. [CrossRef]
6. Wang, Z.; Liu, D.; Yao, Y.; Li, P.; Sun, X.; Feng, D.; Duan, J. Occurrence state of deep coalbed methane: A study considering the co-evolution of stress and pore structure. *Fuel* **2026**, *407*, 137418. [CrossRef]
7. Wei, Q.; Hu, B.; Fang, H.; Zheng, C.; Hou, X.; Gao, D.; Xu, H.; Liu, H.; Shi, C.; Tong, J. Effective Approach with Extra Desorption Time to Estimate the Gas Content of Deep-Buried Coalbed Methane Reservoirs: A Case Study from the Panji Deep Area in Huainan Coalfield, China. *ACS Omega* **2022**, *7*, 11240–11251. [CrossRef] [PubMed]

8. Li, Q.; Zhang, R.; Cai, Y.; Yin, T.; Qiu, F.; Xu, S. CH4 adsorption capacity of coalbed methane reservoirs induced by microscopic differences in pore structure. *Unconv. Resour.* **2024**, *4*, 100097. [CrossRef]
9. Liu, Y.; Hao, C.; Wang, Z.; Xie, J.; Zhao, W.; Meng, F.; Han, Y. Micropore distribution and methane adsorption process and mechanism in bituminous coals: A molecular dynamics simulation study. *J. Environ. Chem. Eng.* **2024**, *12*, 112139. [CrossRef]
10. Esen, O.; Fişne, A. A Comprehensive Study on Methane Adsorption Capacities and Pore Characteristics of Coal Seams: Implications for Efficient Coalbed Methane Development in the Soma Basin, Türkiye. *Rock Mech. Rock Eng.* **2024**, *57*, 6355–6375. [CrossRef]
11. Chen, Z.; Ge, H.; Zhang, J.; Wang, Y.; Yan, Z.; Zhang, Y.; Liang, X. CH4 Adsorption Behavior on Coals with Different Ranks by Grand Canonical Monte Carlo Simulations. *ACS Omega* **2025**, *10*, 53175–53183. [CrossRef]
12. Cheng, Y.; Jiang, H.; Zhang, X.; Cui, J.; Song, C.; Li, X. Effects of coal rank on physicochemical properties of coal and on methane adsorption. *Int. J. Coal Sci. Technol.* **2017**, *4*, 129–146. [CrossRef]
13. Yan, J.; Meng, Z.; Li, G. Diffusion characteristics of methane in various rank coals and the control mechanism. *Fuel* **2021**, *283*, 118959. [CrossRef]
14. Jia, J.; Xing, Y.; Li, B.; Zhao, D.; Wu, Y.; Chen, Y.; Wang, D. Study on the Occurrence Difference of Functional Groups in Coals with Different Metamorphic Degrees. *Molecules* **2023**, *28*, 2264. [CrossRef]
15. Liu, H. Evolution of the Hierarchical Molecular Structures of Tectonically Deformed Coals: Insights from First-Order Raman Spectra. *ACS Omega* **2022**, *7*, 35942–35950. [CrossRef]
16. Yao, S.; Zhang, K.; Jiao, K.; Hu, W. Evolution of Coal Structures: FTIR Analyses of Experimental Simulations and Naturally Matured Coals in the Ordos Basin, China. *Energy Explor. Exploit.* **2011**, *29*, 1–20. [CrossRef]
17. Li, W.; Zhu, Y.-M.; Hu, C.-Q.; Han, S.-B.; Wu, J.-S. Hydrocarbon Generation and Chemical Structure Evolution from Confined Pyrolysis of Bituminous Coal. *ACS Omega* **2020**, *5*, 19682–19694. [CrossRef] [PubMed]
18. Li, Y.; Dai, C.; Meng, S.; Wu, J. Molecular structure characterization of coal with different coalification degrees: A combined study from FT-IR, Raman, ^{13}C NMR spectroscopy and modelling. *J. Mol. Struct.* **2024**, *1310*, 138354. [CrossRef]
19. Wang, C.; Zeng, F.; Li, C.; Xu, Q.; Chen, P. Insight into the molecular structural evolution of a series of medium-rank coals from China by XRD, Raman and FTIR. *J. Mol. Struct.* **2024**, *1303*, 137616. [CrossRef]
20. Mosher, K.; He, J.; Liu, Y.; Rupp, E.; Wilcox, J. Molecular simulation of methane adsorption in micro- and mesoporous carbons with applications to coal and gas shale systems. *Int. J. Coal Geol.* **2013**, *109–110*, 36–44. [CrossRef]
21. Wang, Z.; Zhang, S.; Zhang, X.; Cheng, J.; Lu, W.; Bai, E.; You, Z. Thermodynamic Characteristics of CH4/CO2 Adsorption in Different Rank Coals and Its Molecular Mechanism. *Langmuir* **2025**, *41*, 5419–5438. [CrossRef] [PubMed]
22. Hajianzadeh, M.; Mahmoudi, J.; Sadeghzadeh, S. Molecular dynamics simulations of methane adsorption and displacement from graphenylene shale reservoir nanochannels. *Sci. Rep.* **2023**, *13*, 15765. [CrossRef]
23. Zeng, Q.; Wang, Z.; Sui, T.; Huang, T. Adsorption Mechanisms of High-Pressure Methane and Carbon Dioxide on Coals. *Energy Fuels* **2021**, *35*, 13011–13021. [CrossRef]
24. Si, S.; Wang, Z.; Kang, J.; Guo, W.; Zhang, R.; Peng, C. Mechanism of the influence of high-temperature and high-pressure storage conditions on coal pore structure and methane adsorption kinetics. *Environ. Earth Sci.* **2026**, *85*, 84. [CrossRef]
25. Quan, F.; Lu, W.; Song, Y.; Sheng, W.; Qin, Z.; Luo, H. Multifractal Characterization of Heterogeneous Pore Water Redistribution and Its Influence on Permeability During Depletion: Insights from Centrifugal NMR Analysis. *Fractal Fract.* **2025**, *9*, 536. [CrossRef]
26. Li, Q.; Qin, Y.; Ren, S. Structural characterization analysis and macromolecular model construction of coal from Qinggangping coal mine. *Sci. Rep.* **2023**, *13*, 14365. [CrossRef]
27. Li, S.; Zhu, Y.; Wang, Y.; Liu, J. The Chemical and Alignment Structural Properties of Coal: Insights from Raman, Solid-State 13C NMR, XRD, and HRTEM Techniques. *ACS Omega* **2021**, *6*, 11266–11279. [CrossRef]
28. Yan, J.; Lei, Z.; Li, Z.; Wang, Z.; Ren, S.; Kang, S.; Wang, X.; Shui, H. Molecular structure characterization of low-medium rank coals via XRD, solid state 13C NMR and FTIR spectroscopy. *Fuel* **2020**, *268*, 117038. [CrossRef]
29. Wang, J.; He, Y.; Li, H.; Yu, J.; Xie, W.; Wei, H. The molecular structure of Inner Mongolia lignite utilizing XRD, solid state 13C NMR, HRTEM and XPS techniques. *Fuel* **2017**, *203*, 764–773. [CrossRef]
30. Wang, Z.; Xiong, J.; Zhang, Y.; Tao, G.; Pan, J.; Niu, Q. Investigation of Permeability Stress Induced Damage Evolution of Shallow and Deep Coal Reservoirs in the Junggar Basin, China. *Rock Mech. Rock Eng.* **2026**, *59*, 5065–5092. [CrossRef]
31. Huang, M.; Kang, J.; Li, X.; Liu, X.; Fu, X. Microscopic mechanisms of competitive gas adsorption and diffusion during high volatile bituminous coal CO_2-ECBM process. *Fuel* **2026**, *404*, 136265. [CrossRef]
32. Firouzi, M.; Wilcox, J. Molecular modeling of carbon dioxide transport and storage in porous carbon-based materials. *Microporous Mesoporous Mater.* **2012**, *158*, 195–203. [CrossRef]
33. Liu, Y.; Zhu, Y.; Liu, S.; Li, W. A hierarchical methane adsorption characterization through a multiscale approach by considering the macromolecular structure and pore size distribution. *Mar. Pet. Geol.* **2018**, *96*, 304–314. [CrossRef]

34. *ISO 7404-3-1994*; Methods for the Petrographic Analysis of Bituminous Coal and Anthracite—Part 3: Method of Determining Maceral Group Composition. International Organization of Standards: Geneva, Switzerland, 1994.
35. *ISO 7404-5-1994*; Methods for the Petrographic Analysis of Bituminous Coal and Anthracite—Part 5: Method of Determining Vitrinite Reflectance by Microscopical Methods. International Organization of Standards: Geneva, Switzerland, 1994.
36. *GB/T 212-2008*; Proximate Analysis of Coal. Standardization Administration of China: Beijing, China, 2008.
37. *GB/T 476-1991*; Ultimate Analysis of Coal. Standardization Administration of China: Beijing, China, 1991.

Disclaimer/Publisher's Note: The statements, opinions and data contained in all publications are solely those of the individual author(s) and contributor(s) and not of MDPI and/or the editor(s). MDPI and/or the editor(s) disclaim responsibility for any injury to people or property resulting from any ideas, methods, instructions or products referred to in the content.